NIH Public Access
Author Manuscript
Neuron. Author manuscript; available in PMC 2010 November 12.

Published in final edited form as:
Neuron. 2009 November 12; 64(3): 404–418. doi:10.1016/j.neuron.2009.09.020.

Laminar structure of spontaneous and sensory-evoked population activity in auditory cortex

Shuzo Sakata and **Kenneth D. Harris**
Center for Molecular and Behavioral Neuroscience, Rutgers, The State University of New Jersey, 197 University Avenue, Newark, New Jersey 07102

Summary

Spontaneous activity plays an important role in the function of neural circuits. Although many similarities between spontaneous and sensory-evoked neocortical activity have been reported, little is known about consistent differences between them. Here, using simultaneously recorded cortical populations and morphologically identified pyramidal cells, we compare the laminar structure of spontaneous and sensory-evoked population activity in rat auditory cortex. Spontaneous and evoked patterns both exhibited sparse, spatially localized activity in layer 2/3 pyramidal cells, with densely distributed activity in larger layer 5 pyramidal cells and putative interneurons. However, the propagation of spontaneous and evoked activity differed, with spontaneous activity spreading upward from deep layers and slowly across columns, but sensory responses initiating in presumptive thalamorecipient layers, spreading rapidly across columns. The similarity of sparseness patterns for both neural events, and distinct spread of activity may reflect similarity of local processing, and differences in the flow of information through cortical circuits, respectively.

Introduction

The six-layered structure of the neocortex is one of the most prominent features of the mammalian brain. However, the role of laminar architecture in cortical information processing is still elusive. Pyramidal cells (PCs) – the principal neurons of the neocortex – show strong heterogeneity in morphology, physiology, and gene expression patterns both between and within layers (Douglas and Martin, 2004;Gilbert, 1983;Nelson et al., 2006;Szentagothai, 1983;Thomson and Lamy, 2007). How do these PC populations differ in the strategies they use to encode information? And how does sensory and nonsensory information propagate through such diverse cortical circuits?

Although techniques to record from large neuronal populations are now well established, development of the concepts and quantitative metrics needed to characterize the structure of spiking activity in neuronal populations is still ongoing (Averbeck et al., 2006;deCharms and Zador, 2000;Engel et al., 2001;Harris, 2005;Rieke et al., 1997). One metric that has recently seen increasing attention is *sparseness* (Barlow, 1972;Olshausen and Field, 2004). In a "sparse" representation, signals are represented by the activity of a small fraction of neurons; the other end of this spectrum is a "dense" representation, in which signals are encoded by changes in the firing rates of large numbers of neurons. Recent experimental evidence favors sparse coding

Corresponding author: Kenneth D. Harris, kdharris@andromeda.rutgers.edu, tel: 973-353-3518.

in several cortical regions, in multiple species including rodents (Brecht, 2007;de Kock et al., 2007;Hromadka et al., 2008), monkeys (Vinje and Gallant, 2000) and humans (Bitterman et al., 2008;Quiroga et al., 2005). Furthermore, recordings of individual neurons suggest that the sparseness of sensory-evoked responses may vary between cortical neuronal classes, in multiple sensory cortices (Brecht, 2007;de Kock et al., 2007;Simons, 1978;Swadlow, 1988;Swadlow, 1989;Turner et al., 2005;Wallace and Palmer, 2008;Wu et al., 2008).

The activity of the cortex, however, is not strictly determined by sensory input, and neocortical populations show coordinated, spontaneous patterns of spiking activity in the absence of specific sensory stimuli or motor outputs. Spontaneous neural activity has been best characterized during slow-wave sleep and anesthesia, where it is organized around an alternation of “upstates” of generalized depolarization and spiking, and “downstates” of hyperpolarization and neuronal silence (Hoffman et al., 2007;Steriade et al., 1993). Spontaneous fluctuations in population activity are also observed during quiet wakefulness (Luczak et al., 2007;Luczak et al., 2009;Petersen et al., 2003;Poulet and Petersen, 2008). Patterned spontaneous activity is believed to be important for brain functions such as memory consolidation, behavioral variability, and mental imagery (Fox and Raichle, 2007;Hoffman et al., 2007;Kraemer et al., 2005), as well as pathological phenomena such as auditory hallucinations (Dierks et al., 1999;Hunter et al., 2006).

Recent studies have suggested that the structure of spontaneous population activity in many ways mimics that of sensory responses (Curto et al., 2009;Ganguli et al., 2008;Kenet et al., 2003;Luczak et al., 2009;MacLean et al., 2005). However, given the likely different roles of spontaneous and evoked activity, one might also expect consistent differences between them. One attractive candidate is their structure with respect to cortical layers. Sensory responses are driven mainly through inputs from thalamus, which terminate non-uniformly across layers, with primary thalamic afferents showing a bias in auditory cortex toward lower layer (L) 3 and L4, and the L5/6 border (Kimura et al., 2003;Romanski and LeDoux, 1993;Winer and Lee, 2007). By contrast, spontaneous activity is believed to depend primarily on corticocortical connections (Sanchez-Vives and McCormick, 2000;Timofeev et al., 2000), which have a different laminar profile of termination (Coogan and Burkhalter, 1993;Felleman and Van Essen, 1991;Rouiller et al., 1991). How these anatomical differences affect the laminar structure of spontaneous and evoked population activity is unclear.

Here, we investigate the similarities and differences in laminar structure of evoked and spontaneous population spiking activity in primary auditory cortex of urethane-anesthetized and unanesthetized rats. Spontaneous and evoked firing patterns both exhibited sparse, spatially localized activity in L2/3 pyramidal cells (PCs), with densely distributed activity in larger L5 PCs and putative interneurons (INs). The profile of activity onset across layers, however, varied between the two types of activity, spreading from putative thalamorecipient layers in the case of auditory responses, but upward from deep layers in the case of spontaneous events. These laminar structures of population activity held under both anesthetized and unanesthetized conditions.

Results

In the first set of experiments, we combined large-scale extracellular recordings using silicon multi-site electrodes (‘silicon probes’) (Csicsvari et al., 2003) with simultaneous juxtacellular recording (Pinault, 1996) in urethane-anesthetized rats. We analyzed responses to pure tones of varying frequency and intensity and 1s-long ‘click-trains’ of varying click frequency (Kilgard and Merzenich, 1999;Wang et al., 2008), and spontaneous activity during periods without sound presentation.

Morphologically identified PCs recorded with juxtacellular electrodes (“juxtacells”) were grouped based on somatic location: L2/3 PCs (N=10); L4 PCs (N=10; consistent with a previous report in auditory cortex (Smith and Populin, 2001), PCs were the dominant cell type in L4); L5 PCs (N=28); and L6 PCs (N=6). L5 PCs were further divided into two classes based on apical dendrite diameter: L5 thick PCs (L5 tPCs; apical dendrite diameter>2.5 μm; N=9) and L5 slender PCs (L5 sPCs; apical dendrite diameter<2.5 μm; N=19). Single-units recorded extracellularly with silicon probes (“extracells”) were divided into four groups based on spike waveform and estimated somatic location: out of 1379 extracells, 97 were putatively classified as superficial PCs, 655 as deep PCs, 13 as superficial INs, and 100 as deep INs (see Experimental Procedures and Figures S1-3 for further details; note that to reduce the risk of misclassification, only a subset of extracells were assigned to groups).

Cell-type dependent sparseness of auditory-evoked activity

To investigate whether coding sparseness differs between cell classes, we first characterized the auditory tuning of individual neurons. Figures 1A and B illustrate the tuning of five juxtacells with responses typical of their class (see also Figure S4). In general, L2/3 PCs exhibited highly selective responses in both the spectral and temporal domains, while L5 tPCs were broadly tuned to both stimuli. L4 PCs and L5 sPCs were intermediate between two classes, with L5 sPCs showing heterogeneous response profiles. Intriguingly, L6 PCs showed strikingly different response profiles than other classes, typically without clear frequency-tuned responses (5/6 cells), but sometimes responding to tones and clicks after a ~200ms delay (2/6 cells; Figure 1B). While our juxtacellular recordings did not yield a large enough number of morphologically identified interneurons to perform statistical analyses (N=4), putative INs could be identified in large-scale extracellular recordings by spike waveform (Figure S3). Figure 1C shows the spectral tuning of illustrative putative PCs and INs of superficial and deep layers (see also Figure S5). The firing rates and tuning sharpness of putative PCs did not differ significantly from those of morphologically identified PCs of the corresponding layers (Figure S6); the tuning of putative INs, however, differed from that of PCs, with superficial putative INs showing broader tuning, more similar to deep PCs than to superficial PCs.

The above examples thus suggest that coding sparseness differs between cortical cell classes. We next set out to quantify this impression. Several measures of coding sparseness have been described (Olshausen and Field, 2004;Willmore and Tolhurst, 2001). Because we will later compare the sparseness of evoked responses and spontaneous events, for which standard measures are not applicable, we used a “response probability” measure, defined as the probability that a neuron would fire at least one spike in response to any given stimulus presentation (Figure 2A). For juxtacells, this analysis supported the visual impression conveyed by the example neurons, with L2/3 and L6 PCs showing sparsest activity (i.e. lowest response probabilities), and L5 tPCs the densest activity (i.e. highest response probabilities). For extracells, consistent results were observed: response probability of putative superficial PCs closely matched that of morphologically identified L2/3 PCs, and deep PCs showed response probability intermediate between identified L5 sPCs and tPCs, consistent with the extracellularly recorded population being primarily a mixture of these classes. Putative INs of both layers showed response probability similar to that of deep PCs rather than superficial PCs (Figure 2A). The dependence of response probability on cell class was similar for both tone and click train stimuli (Figure 2B; see **Experimental Procedures**). Analysis of covariance (ANCOVA) revealed that this did not simply reflect a common effect of cell class ($p<0.0001$), suggesting sparseness was correlated between stimulus types even within neurons of a single morphological class. Similar results were obtained using several other sparseness measures (Figure S7).

Sparseness measures do not fully summarize the character of a neuron s sensory tuning; for example, while the measured sparseness of L2/3 and L6 PCs was not significantly different, visual examination of their spectral tuning suggested that L6 PCs (but not L2/3 PCs) carry little information about stimuli during onset periods. To quantify this, we adopted an information-theoretic approach, to estimate how well we could predict the cells' response (i.e., spike count) from the presented tones on single trial basis (Figure 2C; see **Experimental Procedures**). The results of this analysis were again consistent with the examples of Figure 1B: predictability measured in bits per spike was highest in L2/3 PCs (Figure 2C), consistent with sharpest tuning in these neurons; L6 PCs typically carried little information about tone identity (Figure 2C). Thus, we found clear laminar differences in auditory responses, with sparse and more informative activity in L2/3 PCs, and denser activity in larger L5 PCs and putative INs.

Cell-type dependent sparseness of spontaneous activity

We next asked whether the patterns of sparseness described above also apply to spontaneous activity patterns. We began by examining patterns of multi-unit activity (MUA), recorded with linear multisite electrodes (Figure 3A). As previously described (Luczak et al., 2009), spontaneous activity within presumptive L5 consisted of an alternation between periods of network silence ("downstates") and generalized spiking activity ("upstates," see Figure S8 for further information; note that what we refer to as "upstates" are likely to include the "bumps" described by DeWeese and Zador (2004;2006)). Some, but not all upstates visible in deep layers were accompanied by activity in the immediately overlying superficial layers. Figure 3B shows a histogram of normalized MUA rate in both layers during the first 50ms of all detected upstates. For deep layer activity, the histogram had a broad distribution; for superficial layer activity, however, the histogram showed a major peak at 0, confirming that many upstates did not cause measurable superficial spiking activity (see also Figure S9). To investigate the participation of different identified cell classes in upstates, we again used a response probability measure, here defined as the probability a cell would fire at least one spike in any given upstate. A similar pattern of sparseness was seen as for auditory responses, with L2/3 and L6 PCs showing the lowest response probability, and L5 tPCs the highest (Figure 3C). Response probability was correlated on a cell-to-cell basis between spontaneous and auditory-evoked activity (Figure 3D). Again, this did not simply reflect the common effect of cell class on response probability (ANCOVA, $p<0.05$ for tones and upstates; $p<0.05$ for click trains and upstates), suggesting that consistent variations in sparseness both between and within cell classes were preserved in spontaneous and evoked activity.

Difference in propagation of activity across cortical layers

The above analyses showed that the pattern of sparseness across cortical cell classes was similar between evoked and spontaneous activity. However, we observed a clear difference between these two types of events in the propagation of activity between layers. Figure 4A shows examples of laminar MUA traces during successive evoked and spontaneous spiking events. At the onset of auditory responses, activity originated in the upper middle and a part of deep layers, locations which also corresponded to the locations of early sinks revealed by current source density (CSD) analysis (Figure S10). Activity at upstate onset, however, was first seen in the deep layers and spread upward (Figure 4A). To quantify the difference between these patterns, we computed a "peak latency" measure, defined as median MUA spike time in a 50ms window after event onset, as a function of putative laminar location (Figures 4B and C; for different measures of latency see Figure S11). This analysis confirmed a significant difference in laminar temporal profile between the onset of upstates and auditory-evoked responses (Figure 4C). The observed laminar profile of auditory responses was similar across responses to clicks and multiple tone frequencies and intensities that evoked spiking responses (Figure S12), as well as between experiments (Figure S10).

Spatial- and laminar-dependence of correlated activity

The results described above focused on the properties of individual neurons, and the coordination of neurons within a single cortical column, but not the organization of activity across multiple columns. For example, sparse firing of superficial PCs could reflect either spatially localized or distributed activity (Figure 5A). Because primary auditory cortex is tonotopically organized (Schreiner et al., 2000), we expected that for tone responses, activity should be spatially localized; however, the spatial structure of click responses and upstates, and the organization of trial-to-trial response variations was not obvious *a priori*.

To address this issue, we used spike-sorted extracellular population activity recorded from multi-shank silicon probes (Figure 5B). Visual examination of rasters suggested spiking activity in superficial layers to be locally clustered compared with deep layers, for upstates as well as responses to tones and clicks (Figure 5B). To quantify this impression, we performed a correlation analysis on spike counts in the 50ms period following event onsets (Figure 5C). For upstates, correlations between pairs of superficial cells were much stronger for local pairs recorded from the same shank (estimated spacing <~50μm)(Henze et al., 2000) than for distal pairs from separate shanks (estimated spacing >~ 200μm); in deep layers, however, there was only a subtle difference between local and distal correlations. For sensory coding, two types of correlations are typically distinguished: similarity of average tuning curves ("signal correlations"), and correlated variability between response to repetitions of a particular stimulus ("noise correlations") (Averbeck et al., 2006;Gawne and Richmond, 1993). For all correlation types, a qualitatively similar pattern was observed as for upstates: in superficial layers, correlations were stronger for local than distal pairs, while in deep layers, there were only subtle differences between local and distal correlations (Figure 5C).

Spatiotemporal dispersion of evoked and spontaneous activity

The spatial dependence of cell-to-cell correlations was therefore consistent with sparse, spatially localized activity in L2/3, occurring on top of broader activity in L5. To confirm this possibility more directly, we employed a different experimental approach (Figure 6A), in which multisite electrodes were inserted parallel to the layers of auditory cortex. Figures 6B and C show examples of MUA traces recorded with this approach, for upstates and evoked responses, respectively. There was considerable variability between events in the set of sites at which activity was induced, particularly in the superficial layers. Consistent with the correlation analyses described above, activity was more spatially localized in superficial than in deep layers, which was statistically confirmed by a measure of spatial dispersion (Figure 6D). In addition, the speed with which activity spread across recording sites was on average faster for evoked events than for upstates, consistent with the tendency for the latter to sometimes propagate as traveling waves (Luczak et al., 2007;Petersen et al., 2003) (Figures 6E and S13).

Sparseness and propagation of population activity in unanesthetized animals

To determine how well the above results, collected under urethane anesthesia, generalized to unanesthetized animals, we performed further recordings using silicon probes in head-restrained, unanesthetized rats (N=7; see **Experimental Procedures**). Out of 235 spike-sorted single units, we identified 48 putative superficial PCs, 121 putative deep PCs, 4 putative superficial INs, and 14 putative deep INs. Because the number of recorded superficial INs was too small for statistical analysis, we pooled these two IN populations for further analysis. Consistent with previous results (Luczak et al., 2007;Petersen et al., 2003;Poulet and Petersen, 2008), we observed coordinated spontaneous fluctuations of population activity in this data (Figure 7A). Also consistent with a recent study (Greenberg et al., 2008), we noticed several quantitative differences in neuronal activity between unanesthetized and urethane-anesthetized conditions including higher mean firing rates and weaker spontaneous correlations in superficial and deep layers (Figure S14).

To gauge whether our main observations under anesthesia generalized to this dataset, we repeated the analyses described above. First, we investigated the cell-type dependent sparseness of both auditory-evoked and spontaneous activity (Figures 7B-D). As under anesthesia, visual examination of spectral tuning suggested sharper tuning of superficial PCs than deep PCs (Figure 7B), which was statistically confirmed using the response probability measure (Figure 7C). Putative INs showed higher response probability than both classes of putative PCs. Similar results were found for click-evoked responses and spontaneous events, and also confirmed using other measures of sparseness (Figure S15). Moreover, response probability was correlated on a cell-to-cell basis between events (Figure 7D; ANCOVA, $p < 0.01$ in all cases; c.f. Figures 2B and 3D). Thus, although firing rates were higher for all cell classes in the unanesthetized data, the relative pattern of sparseness between cell classes was similar in both cases.

Second, examination of the laminar profile of evoked and spontaneous activity onset across layers suggested a pattern similar to that found under anesthesia, with spontaneous events spreading upward from deep layers, and auditory evoked activity originating in the upper middle and a part of deep layers (Figure 8A). This impression was statistically confirmed using the “peak latency” measure (Figures 8B,C; c.f. Figure 4); also similarly to the anesthetized case, the laminar locations of earliest stimulus-evoked spiking corresponded to early current sinks as revealed by CSD analysis (Figure S16).

Finally, analysis of data collected with electrodes parallel to the cortical laminae (N=2) confirmed that the spatial dispersion of population activity in superficial layers was narrower compared to deep layers (Figures 8D,E; c.f. Figure 6). The spread of activity across cortical columns was also faster for evoked activity (120.5 ± 5.1 mm/sec in superficial layers; 100.3 ± 4.9 mm/sec in deep layers) than spontaneous events in the corresponding layers (54.0 ± 9.5 mm/sec in superficial layers; 65.5 ± 5.1 mm/sec in deep layers) (ANOVA and post-hoc lsd test, $p<0.01$). Thus, while we found quantitative differences between anesthetized and unanesthetized conditions, our experiments suggested the general laminar structure of evoked and spontaneous activity was similar in both cases.

Discussion

We compared the laminar structure of evoked and spontaneous population activity in primary auditory cortex. Common to both types of activity was a laminar and cell type-dependent variation in sparseness, with sparse spatially clustered activity in PCs of superficial layers and distributed dense activity in the deep layers, with densest firing in large L5tPCs and putative INs. Spontaneous and evoked activity differed, however, in the spread of activity across layers and columns, with sensory-evoked activity showing earliest activation in putative thalamorecipient layers and rapid spread across cortical columns, but spontaneous patterns spreading upward from deep layers, and spreading more slowly between columns. These patterns are summarized in Figure 9.

Comparison with previous studies

Laminar organization has been studied in a large number of cortical areas and species, using a variety of stimulus paradigms, animal conditions (e.g., anesthetized or unanesthetized), and experimental methods to identify particular neuronal classes, posing challenges for direct comparison of different data sets. The combination of juxtacellular and large-scale extracellular recording used here has, to our knowledge, not yet been applied in any sensory modality. However, several previous recordings of single-neuron sensory responses appear consistent with our findings, in particular regarding sparser activity in superficial PCs, denser activity in large or subcortically projecting L5 PCs, and differences between superficial PCs and INs (Brecht et al., 2003;Brecht, 2007;de Kock et al., 2007;Sohya et al., 2007;Swadlow, 1988;Swadlow, 1989;Swadlow, 1994;Turner et al., 2005;Wallace and Palmer, 2008;Wu et al., 2008). Of particular interest, however, is a recent study by Hromadka et al (2008), who used cell-attached recording techniques in auditory cortex of unanesthetized rats, but reported only modest differences in spontaneous and evoked responses across layers. We suggest that one or more of three factors may contribute to this apparent discrepancy. First, while our study used adult rats (several months old), Hromadka et al used juveniles (younger than one month). Second, although it is unlikely that anesthesia itself is a sufficient explanation (we found a consistent laminar profile of sparseness in both anesthetized and unanesthetized animals), it remains possible that differences in age or training paradigm led to differences in the attentional or cognitive state of the unanesthetized subjects in the two studies. Finally, while both studies reported denser activity in narrow-spiking putative INs than putative PCs, their depth analysis was based on the full population of morphologically unreconstructed neurons, suggesting that the lack of reported depth tuning might result from the inclusion of densely-firing superficial INs, in addition to sparsely-firing superficial PCs.

Cortical activity has been studied with optical imaging methods, which primarily reflect activity in the superficial layers. Our conclusion of sparse, spatially localized activity in superficial layers might at first appear to conflict with voltage-sensitive dye (VSD) studies, which show both sensory-evoked and spontaneous events spreading over large areas of the sensory cortical surface (Ferezou et al., 2007;Kenet et al., 2003;Petersen et al., 2003). We note however that VSD imaging reflects subthreshold depolarization rather than supratheshold spiking. Indeed, simultaneous imaging of voltage- and calcium-sensitive dyes (which primarily reflect suprathreshold spiking) indicates that suprathreshold activity is spatially localized within the somatosensory cortex, compared to subthreshold activation (Berger et al., 2007). We speculate that the widespread distribution of superficial subthreshold activity seen with VSD might correspond more closely with the distribution of spiking in the deep layers, and that deep-to-superficial intracolumnar projections might contribute to the broad distribution of subthreshold depolarization reported in superficial layers.

More generally, while a number of prior studies have described similarities in the structure of spontaneous and evoked activity (e.g. Kenet et al., 2003;Luczak et al., 2009;MacLean et al., 2005), we are not aware of previous reports of consistent differences between these two types of activity. We suggest however that differential flow of activity between layers was unlikely to have been found in these previous studies, which studied only populations within single layers, either due to the use of surface optical imaging (Kenet et al., 2003), or a focus on L4 (MacLean et al., 2005), or extracellular electrodes located in deep layers (Luczak et al., 2009). The picture of Figure 9 therefore appears broadly consistent with studies using multiple techniques in multiple cortical areas, perhaps suggesting a mode of operation of cortical laminar circuits that might be common across multiple sensory regions.

Possible mechanisms for laminar-dependent patterns of activity

What mechanisms could account for the differing patterns of activity in superficial and deep layers? In the case of pure tone stimuli, given the facts of tonotopic organization, and sharper tuning in superficial than deep layer PCs, one would predict a spatial distribution similar to that outlined in Figure 9. However, the fact that a similar distribution is also seen for click responses, spontaneous upstates, and noise correlations suggests that the same mechanisms that cause layer-dependent frequency tuning might also shape layer-dependent sparseness patterns in more general circumstances. Although it is not yet possible to give a firm answer to what these mechanisms are, *in vitro* work in auditory and other sensory cortices suggests a number of potential candidates. While lateral excitatory connections in deep layers are typically strong and widespread (Feldmeyer et al., 2006;Schubert et al., 2007;Thomson and Lamy, 2007), the probability of PC-PC connections in L2/3 significantly decays over a spatial scale of ~150 m (Holmgren et al., 2003;Oswald and Reyes, 2008), providing a potential mechanism for local clustering of superficial spiking activity at this scale. Furthermore, inhibitory inputs have been reported stronger onto L2/3 PCs than L5 PCs (van Brederode and Spain, 1995), with thick L5 PCs – for which we observed the densest activity – receiving weaker inhibition than slender PCs (Hefti and Smith, 2000). Layer-specific features of excitatory and inhibitory circuits such as these may impose a consistent laminar structure on all population activity patterns, whether evoked by auditory stimuli, or occurring spontaneously.

The finding that evoked and spontaneous activity onsets propagate differently across cortical layers suggests that these types of activity are triggered by different mechanisms *in vivo*. Afferents from the ventral medial geniculate nucleus to primary auditory cortex terminate most densely in two laminar bands corresponding to lower L3/L4, and the L5/6 boundary (Kimura et al., 2003;Romanski and LeDoux, 1993). We found that the earliest sensory-evoked responses are found in the middle layers and a restricted portion of the lower layers, which correspond on an experiment-to-experiment basis with the locations of early sinks measured by CSD analysis (Figures S10 and S16) (see also Kaur et al., 2005). Our data are therefore consistent with an initiation of sensory-evoked activity in the thalamorecipient layers. We note that PCs can receive excitatory inputs all along their dendritic length, and that thalamic inputs could in principle provide excitation to neurons of other laminae (Bureau et al., 2006). Earlier sensory responses in cells of thalamorecipient layers might however reflect these cells receiving stronger excitatory drive, perhaps due to excitation proximal to the soma. While we observed spontaneous activity to often spread as a traveling wave (Luczak et al., 2007), sensory responses appeared closer to simultaneously across the cortical surface. This pattern of sensory responses is therefore consistent with divergent and broadly tuned thalamocortical input, a result also suggested by the persistence of broadly tuned responses after inhibition of spiking in auditory cortex (Liu et al., 2007). The observed spread of upstates is consistent with *in vitro* models, which show generation and spread of spontaneous activity in deep layers (Sanchez-Vives and McCormick, 2000). Deep layers are a major target of “feedback” projections from higher cortical areas (Felleman and Van Essen, 1991;Rouiller et al., 1991). The fact that auditory cortical upstates were first seen in deep layers is thus consistent with a role of projections from higher cortical regions in initiating spontaneous patterns in primary sensory cortex, consistent with their proposed role in processes such as memory replay (Buzsaki, 1989;Hoffman et al., 2007;Ji and Wilson, 2007;Marr, 1971).

Functional implications of laminar-dependent population activity

Theoretical studies suggest that sparse coding has many advantages for neuronal computation, including energy efficiency, and information storage through synaptic plasticity (Barlow, 1972;Levy and Baxter, 1996;Marr, 1969;Olshausen and Field, 2004). Nevertheless, sparse coding comes at a cost, due to the large number of cells needed to support sparse codes. This cost may be particularly acute for physically larger cells such as those that give rise to long-range projections. One potential solution to this dilemma might be for neuronal circuits to employ sparse coding in a large number of small neurons, and for this information to be integrated by a smaller number of large densely-coding cells that broadcast the results of local computations to distant structures. Such a scheme is proposed to operate in mammalian cerebellum (Marr, 1969) and hippocampal formation (Barnes et al., 1990), as well as the invertebrate olfactory system (Laurent, 2002). Our results suggest that similar principles may apply in auditory cortex: large L5tPCs, which show densest coding, form the principal subcortical output (Ojima et al., 1992), whereas the smaller L2/3PCs employ the sparsest coding.

What functional consequences might the difference in propagation of spontaneous and sensory-evoked activity between layers have? If it is true that spontaneous activity corresponds to "replay" of previous sensory experiences (Hoffman et al., 2007;Ji and Wilson, 2007), then our results suggest that the original and replayed patterns may differ in timing with regards to populations of different layers. Although the timing differences will be subtle – of the order tens of milliseconds – spike timing differences of this magnitude can have a dramatic effect on the existence and sign of synaptic changes (Caporale and Dan, 2008), with a further dependence on the laminar location of dendritic inputs (Froemke et al., 2005;Kampa et al., 2007). Consistent laminar timing differences might thus imply different consequences of the original and replayed activity for the plasticity of interlaminar synapses, perhaps consistent with a proposed function of sleep in both consolidation and erasure of traces formed during learning (Buzsaki, 1989;Crick and Mitchison, 1983).

Experimental Procedures

Surgical procedures

Fifty-nine adult Spargue-Dawley rats (range 200–517 g, both sexes) were used for the experiments. All procedures were approved by the Institutional Animal Care and Use Committee of Rutgers University. Animals were anesthetized with 1.5 g/kg urethane. An additional solution was administered to reduce brain edema (dexamethasone, 0.10 mg). Lidocaine (2%, 0.10 – 0.20 mg) was also administered subcutaneously at the site of incision. Additional doses of urethane (~0.2 g/kg) were given if necessary. The animal was placed in a custom naso-orbital restraint that left the ears free and clear. Body temperature was retained at 37 °C with a feedback temperature controller (FHC). After reflecting the temporalis muscle, left auditory cortex was exposed via craniotomy and a small duratomy was carefully performed. The skull cavity was filled with warm saline during surgery. During recording, the cavity was filled with 1– 1.5 % agar/0.1 M phosphate buffered saline (PBS) to reduce pulsation.

Auditory stimulation

Acoustic stimuli were generated digitally (sampling rate 97.7 kHz, TDT3, Tucker-Davis Technologies) and delivered in free-field through a calibrated electrostatic loudspeaker (ES1, Tucker-Davis Technologies) located ~10 cm in front of the animal, in a single-walled soundproof box (Industrial Acoustics Company) with the interior covered by 3 inches of acoustic absorption foam. Calibration was conducted using a pressure microphone (ACO-7017, ACO Pacific) close to the animal's right ear. Acoustic stimuli consisted of short pure tones (50ms long with 5ms cosine ramps, 1/6 or 1/8 octave steps, 3–48kHz, 10 dB steps, 0–80 dB SPL), long pure tones (400 to 1000ms long with 5ms cosine ramps, 1 or 1/3 octave steps, 3–48kHz, 30 and 70 dB SPL), and 1sec long repetitive click trains (5ms broadband noise with 1ms cosine ramps, 2–50 Hz at 80dB SPL). Other stimuli (sinusoidal amplitude-modulated broadband noises and 3ms square pulse clicks) were also presented in a subset of experiments, but not used in the current analyses.

Simultaneous juxtacellular and large-scale extracellular recordings

Neuronal activity in the auditory cortex was recorded simultaneously with a 16 or 32 channel "silicon probe" (NeuroNexus Technologies), and a glass electrode for recording individual morphologically identified neurons. Pipettes were pulled from glass capillaries (World Precision Instruments) using a vertical puller (Narishige, PE-2 or PC-10) and the pipette tip was broken under a microscope. Pipettes were filled with 1.5–2.0 % Neurobiotin (Vectastain) dissolved in 0.5M NaCl. Their resistance was 10–20 MΩ *in vivo*. Broadband signals (> 1 Hz) from the silicon probe were amplified (1000x) (Plexon, PBX2), and narrow-band signals (100 Hz - 3 KHz) from the pipette were amplified (1000x) with a MultiClamp 700B (Molecular Devices). All data were digitized at 20 kHz and stored for offline analysis. For histological verification of tracks (Figure S2A), the rear of probes was painted with DiI (Invitrogen, D-282, ~10% in ethanol). Recording was followed by juxtacellular labeling: positive current pulses

(0.5–8nA, 50% duty cycle) were applied at 2 or 5 Hz. The current was slowly increased until it drove the discharge activity. After that, the current was immediately adjusted at 0.5–2nA and then this rhythmic activity was maintained for up to 20 min. Several penetrations were made per animal.

Histology

Histological procedures—After electrophysiological experiments and a survival period (30 min to 6 hr), rats were perfused transcardially with physiological saline followed by 4% paraformaldehyde plus 0.5 % glutaraldehyde/0.1 M phosphate buffer, pH 7.4. After a 12–14 h postfixation in the same fixative without glutaraldehyde, brains were cut into 80 μm coronal sections with a microtome (Leica), and the sections collected and placed in 0.1 M PBS. For verification of silicon probe tracks, the free-floating sections were counterstained with NeuroTrace (1:80; Invitrogen) in PBS for 20 min at room temperature. For visualization of juxtacellularly labeled cells, the free-floating sections were incubated in PBS containing 0.3% H_2O_2 for 20 min at room temperature, then processed with an avidin-biotinylated horseradish peroxidase complex (1:100; Vectastain ABC Elite kit) in PBS with 0.2% Triton X-100 at room temperature for 2.5 hrs or at 4 °C overnight. The reaction was visualized with nickel-enhanced coloring solution (0.2 mg/mL daminobenzidine: DAB, 0.03% H_2O_2, 0.03% nickel chloride in tris-buffered saline). The sections were mounted on gelatin-coated slides, dehydrated, and embedded in a mixture of Distyrene, a plasticizer, and xylene (DPX Mountant) (Fisher Scientific). Selected sections were also counterstained with cresyl violet or thionin to visualize laminar structure.

Histological analysis—Juxtacells were identified morphologically as PCs by pyramidal shape soma and a prominent apical dendrite (Figures 1A and S1). Laminar borders were determined based on background staining and/or Nissl counterstain under microscope. Adobe Photoshop was used for 2D reconstructions. To quantify morphological features, only the peri-somatic region was reconstructed (analyzed with Neurolucida and Neurolucida Explorer; MicroBrightField, Inc.). Relative depth of soma (Figure S1) was calculated as D/T, where D is the somatic depth from the cortical surface and T is cortical thickness. Dendritic diameter was defined as the apical dendrite diameter 10μm from the center of somatic contour.

Spike train analysis

Spike detection and sorting—All spike detection and sorting took place off-line. For spike sorting, freely available software was used (KlustaKwik, http://klustakwik.sourceforge.net; Klusters, http://klusters.sourceforge.net) (Harris et al., 2000;Hazan et al., 2006). Unit isolation quality was assessed by "isolation distance" (Harris et al., 2001;Schmitzer-Torbert et al., 2005); only cells with values ≥20 were further analyzed (Figure S2). Cells were classified as putative PCs and INs based on mean waveform (Figure S3) (Sirota et al., 2008).

Depth estimation of extracells—The depth of spike-sorted units ("extracells") was estimated from the stereotaxically-estimated depth of the electrode tip and spike waveform profiles. Somatic location was estimated as the recording site with mean waveform of maximum peak-to-trough amplitude. Putative superficial layers (L2/3) and deep layers (L5) were defined as 0–500μm and 800–1100μm from surface, respectively. Note that to reduce the risk of misclassification (such as might arise from somatodendritic backpropagation of action potentials in large pyramidal cells; Buzsaki and Kandel, 1998), this criterion was deliberately conservative, with cells of intermediate depth or deeper than putative L5 not assigned to either group for further analysis. Dimpling of cortical surface was not corrected.

Analysis for responses to click trains—Spike counts were computed for a 50ms window following each click of each frequency click train. Sparseness and pairwise correlations were computed by treating each click of each train frequency as a separate stimulus; note that this analysis may therefore be insensitive to non-synchronous click responses (Wang et al., 2008). Click trains of >20Hz were not used for this analysis, due to window overlap.

Information-theoretic analysis—To estimate how well a neuron s firing rate could be predicted from the tone presented, we used a cross-validation approach, which provides a lower-bound estimate of the cells information content (Harris et al., 2003;Itskov et al., 2008;Kjaer et al., 1994). Estimates were based on spike counts in a 50ms time window after each tone onset. Probability distributions for spike counts were estimated from the training set using the two-parameter generalized Poisson distribution (Consul and Jain, 1973):

$$p(x;\lambda_1,\lambda_2)=\lambda_1(\lambda_1+x\lambda_2)^{x-1}e^{-(\lambda_1+x\lambda_2)}/x!$$

where x is the spike count and λ_1 and λ_2 are parameters. This was used rather than the classical Poisson as it allows fitting distributions whose variance exceeds their mean. Note that if λ_2=0 this reduces to the standard Poisson with parameter λ_1. To fit the parameters of the Generalized Poisson distribution, we used the method of moments (Consul and Jain, 1973):

$$\lambda_2=1-\sqrt{\mu/V}\cdot\quad\lambda_1=\mu(1-\lambda_2)$$

where μ and V are the mean and variance of the spike count distribution being fit. Information was estimated for each cell as the mean over the test set of the $\log_2$ likelihood ratio of the observed spike counts under conditional and marginal distributions fit from the training set, normalized by test set spike count:

$$\widehat{I}=\frac{1}{N_{\text{spikes}}}\sum_{\text{t}\in\text{test set}}\log_2\left(\frac{p\left(x_t;\lambda_1\left(s_t\right),\lambda_2\left(s_t\right)\right)}{p\left(x_t;\lambda_1{}^0,\lambda_2{}^0\right)}\right)$$

where s_t denotes the stimulus presented on test set trial t; x_t is the number of spikes fired on test set trial t; $\lambda_1(s)$ and $\lambda_2(s)$ are the parameters of the conditional distribution estimated from the training set for stimulus s; $\lambda_1^0$and λ_2^0 are the parameters of the marginal distribution estimated using the method of moments from all training set trials (regardless of stimulus); and N_{spikes} is the total number of test set spikes (to produce a result measured in bits/spike). Because we used cross-validation, overfitting could only result in underestimates of the information; to reduce the amount of underestimation we used a regularization procedure, fitting the parameters $\lambda_1(s)$ and $\lambda_2(s)$ of the conditional distributions to a weighted sum of the conditional and marginal mean and variance: $(1-a)\,\mu_s + a\mu_0$ and $(1-a)\,V_s + aV_0$, where μ_s, V_s are the mean and variance of training set spike counts for stimulus s; μ_0, V_0 are the mean and variance of training set spike counts over all stimuli; and a is a regularization parameter. Note that if a=0, no regularization is performed, whereas if a=1 the conditional and marginal distributions will be equal and the estimated information will be 0. For each cell, information was computed for a=0, 0.1, 0.2, … 1.0, and the value giving maximal cross-validated information chosen.

Upstate detection—The method used to detect upstate onsets is illustrated in Figure S8. Upstates were detected from the smoothed MUA (summed population activity, smoothed with a 10ms Gaussian kernel), during periods without stimulus presentation. Upstate onsets were defined as times when the smoothed MUA crossed above a threshold defined as the geometric mean of MUA over all spontaneous activity, after a period of at least 100ms in which mean

MUA rate was below 0.2 the threshold value. Only upstates for which mean MUA over a 200ms window after onset remained above threshold were further analyzed.

Estimation of spatial spread and propagation speed—To estimate the spatial dispersion of a population pattern recorded with multishank linear electrodes (Figure 6D), we first computed for each event the MUA spike count in a 50ms window, as a function of electrode location (50μm spacing). For each event we thus obtained a probability distribution over recording sites, for the location of recorded spikes. The spatial dispersion was defined to be the inter-quartile range of this distribution, i.e. the distance between the locations of the electrodes corresponding to the 25th and 75th percentiles.

To estimate propagation speed across cortical columns, we first computed the median MUA spike time in a 50ms window after event onset, for each recording site. Speed was estimated by linear regression of this median time against recording site (Luczak et al., 2007). Only events where the regression was statistically significant (p<0.05) were used (see also Figure S13).

Recording from head-restrained animals

Seven additional adult rats (range 270–380 g, male) were recorded under head-restrained, unanesthetized conditions. In initial surgery, animals were anesthetized by ketamine (100 mg/kg) and xylaxine (10 mg/kg), and placed in a stereotaxic apparatus (David Kopf Instruments). A head-post (Thorlabs, Inc.) was attached with dental cement (3M ESPE, RelyX Luting Cement), and the left temporal muscle removed and covered with biocompatible glue and dental cement. After a recovery period (>48hr, during which antibiotics were given), animals were lightly water-deprived, and handling (5–10 min/day) and head-fixation training began. Training was performed for at least 5 sessions (Figure S14A), during which the duration of restraint was gradually extended. 10% sucrose was frequently given during training and water was freely available for one hour after daily training. To familiarize the animal with the sounds to be presented during the recording session, these were presented in the last several training sessions. On the day of recording, craniotomy and duratomy were carefully performed under anesthesia (0.8–5% isoflurane). Neither skin nor muscle was cut during this surgery. After a recovery period (>1hr), recording began. During recording, animals were video-monitored online, displaying quiet immobility with eyes open or closed, and occasional periods of whisking and grooming; data was not divided by behavior before analysis, suggesting that our datasets were likely to be mixture of multiple behavioral states. If animals showed discomfort, experiments were immediately terminated. Recording sessions usually lasted 1–2hrs. All training and recordings were performed in the soundproof box mentioned above.

Supplementary Material

Refer to Web version on PubMed Central for supplementary material.

Acknowledgments

We thank S. Marguet, P. Bartho, T. Klausberger, A. Luczak and N. Lee for outstanding technical advice and assistance; G. Buzsaki, D. Pare, P. Chadderton, A. Renart and J. de la Rocha for their generous support, advice, and comments on the manuscript; B. Krekelberg and members of the Harris lab for discussion. This work was supported by NIH (MH073245 and DC009947), NSF (SBE-0542013 to the Temporal Dynamics of Learning Center, an NSF Science of Learning Center), the Alfred P Sloan Foundation to K.D.H, and the Japan Society for the Promotion of Science Postdoctoral Fellowships for Research Abroad and the Sound Technology Foundation to S.S.

References

Averbeck BB, Latham PE, Pouget A. Neural correlations, population coding and computation. Nat Rev Neurosci 2006;7:358–366. [PubMed: 16760916]

Barlow HB. Single units and sensation: a neuron doctrine for perceptual psychology? Perception 1972;1:371–394. [PubMed: 4377168]

Barnes CA, McNaughton BL, Mizumori SJ, Leonard BW, Lin LH. Comparison of spatial and temporal characteristics of neuronal activity in sequential stages of hippocampal processing. Prog Brain Res 1990;83:287–300. [PubMed: 2392566]

Berger T, Borgdorff A, Crochet S, Neubauer FB, Lefort S, Fauvet B, Ferezou I, Carleton A, Luscher HR, Petersen CC. Combined voltage and calcium epifluorescence imaging in vitro and in vivo reveals subthreshold and suprathreshold dynamics of mouse barrel cortex. J Neurophysiol 2007;97:3751–3762. [PubMed: 17360827]

Bitterman Y, Mukamel R, Malach R, Fried I, Nelken I. Ultra-fine frequency tuning revealed in single neurons of human auditory cortex. Nature 2008;451:197–201. [PubMed: 18185589]

Brecht M. Barrel cortex and whisker-mediated behaviors. Curr Opin Neurobiol 2007;17:408–416. [PubMed: 17702566]

Brecht M, Roth A, Sakmann B. Dynamic receptive fields of reconstructed pyramidal cells in layers 3 and 2 of rat somatosensory barrel cortex. J Physiol 2003;553:243–265. [PubMed: 12949232]

Bureau I, von Saint PF, Svoboda K. Interdigitated paralemniscal and lemniscal pathways in the mouse barrel cortex. PLoS Biol 2006;4:e382. [PubMed: 17121453]

Buzsaki G. Two-stage model of memory trace formation: a role for "noisy" brain states. Neuroscience 1989;31:551–570. [PubMed: 2687720]

Buzsaki G, Kandel A. Somadendritic backpropagation of action potentials in cortical pyramidal cells of the awake rat. J Neurophysiol 1998;79:1587–1591. [PubMed: 9497436]

Caporale N, Dan Y. Spike timing-dependent plasticity: a Hebbian learning rule. Annu Rev Neurosci 2008;31:25–46. [PubMed: 18275283]

Consul PC, Jain GC. A generalization of the Poisson distribution. Technometrics 1973;15:791–799.

Coogan TA, Burkhalter A. Hierarchical organization of areas in rat visual cortex. J Neurosci 1993;13:3749–3772. [PubMed: 7690066]

Crick F, Mitchison G. The function of dream sleep. Nature 1983;304:111–114. [PubMed: 6866101]

Csicsvari J, Henze DA, Jamieson B, Harris KD, Sirota A, Bartho P, Wise KD, Buzsaki G. Massively parallel recording of unit and local field potentials with silicon-based electrodes. J Neurophysiol 2003;90:1314–1323. [PubMed: 12904510]

Curto C, Sakata S, Marguet S, Itskov V, Harris KD. A simple model of cortical dynamics explains variability and state-dependence of sensory responses in urethane-anesthetized auditory cortex. J Neurosci 2009;29:10600–10612. [PubMed: 19710313]

de Kock CP, Bruno RM, Spors H, Sakmann B. Layer- and cell-type-specific suprathreshold stimulus representation in rat primary somatosensory cortex. J Physiol 2007;581:139–154. [PubMed: 17317752]

deCharms RC, Zador A. Neural representation and the cortical code. Annu Rev Neurosci 2000;23:613–647. [PubMed: 10845077]

Deweese MR, Zador AM. Shared and private variability in the auditory cortex. J Neurophysiol 2004;92:1840–1855. [PubMed: 15115790]

Deweese MR, Zador AM. Non-Gaussian membrane potential dynamics imply sparse, synchronous activity in auditory cortex. J Neurosci 2006;26:12206–12218. [PubMed: 17122045]

Dierks T, Linden DE, Jandl M, Formisano E, Goebel R, Lanfermann H, Singer W. Activation of Heschl's gyrus during auditory hallucinations. Neuron 1999;22:615–621. [PubMed: 10197540]

Douglas RJ, Martin KA. Neuronal circuits of the neocortex. Annu Rev Neurosci 2004;27:419–451. [PubMed: 15217339]

Engel AK, Fries P, Singer W. Dynamic predictions: Oscillations and synchrony in top-down processing. Nat Rev Neurosci 2001;2:704–716. [PubMed: 11584308]

Feldmeyer D, Lubke J, Sakmann B. Efficacy and connectivity of intracolumnar pairs of layer 2/3 pyramidal cells in the barrel cortex of juvenile rats. J Physiol 2006;575:583–602. [PubMed: 16793907]

Felleman DJ, Van Essen DC. Distributed hierarchical processing in the primate cerebral cortex. Cereb Cortex 1991;1:1–47. [PubMed: 1822724]

Ferezou I, Haiss F, Gentet LJ, Aronoff R, Weber B, Petersen CC. Spatiotemporal dynamics of cortical sensorimotor integration in behaving mice. Neuron 2007;56:907–923. [PubMed: 18054865]

Fox MD, Raichle ME. Spontaneous fluctuations in brain activity observed with functional magnetic resonance imaging. Nat Rev Neurosci 2007;8:700–711. [PubMed: 17704812]

Froemke RC, Poo MM, Dan Y. Spike-timing-dependent synaptic plasticity depends on dendritic location. Nature 2005;434:221–225. [PubMed: 15759002]

Ganguli S, Bisley JW, Roitman JD, Shadlen MN, Goldberg ME, Miller KD. One-dimensional dynamics of attention and decision making in LIP. Neuron 2008;58:15–25. [PubMed: 18400159]

Gawne TJ, Richmond BJ. How independent are the messages carried by adjacent inferior temporal cortical neurons? J Neurosci 1993;13:2758–2771. [PubMed: 8331371]

Gilbert CD. Microcircuitry of the visual cortex. Annu Rev Neurosci 1983;6:217–247. [PubMed: 6132585]

Greenberg DS, Houweling AR, Kerr JN. Population imaging of ongoing neuronal activity in the visual cortex of awake rats. Nat Neurosci 2008;11:749–751. [PubMed: 18552841]

Harris KD. Neural signatures of cell assembly organization. Nat Rev Neurosci 2005;6:399–407. [PubMed: 15861182]

Harris KD, Csicsvari J, Hirase H, Dragoi G, Buzsaki G. Organization of cell assemblies in the hippocampus. Nature 2003;424:552–556. [PubMed: 12891358]

Harris KD, Henze DA, Csicsvari J, Hirase H, Buzsaki G. Accuracy of tetrode spike separation as determined by simultaneous intracellular and extracellular measurements. J Neurophysiol 2000;84:401–414. [PubMed: 10899214]

Harris KD, Hirase H, Leinekugel X, Henze DA, Buzsaki G. Temporal interaction between single spikes and complex spike bursts in hippocampal pyramidal cells. Neuron 2001;32:141–149. [PubMed: 11604145]

Hazan L, Zugaro M, Buzsaki G. Klusters, NeuroScope, NDManager: a free software suite for neurophysiological data processing and visualization. J Neurosci Methods 2006;155:207–216. [PubMed: 16580733]

Hefti BJ, Smith PH. Anatomy, physiology, and synaptic responses of rat layer V auditory cortical cells and effects of intracellular GABA(A) blockade. J Neurophysiol 2000;83:2626–2638. [PubMed: 10805663]

Henze DA, Borhegyi Z, Csicsvari J, Mamiya A, Harris KD, Buzsaki G. Intracellular features predicted by extracellular recordings in the hippocampus in vivo. J Neurophysiol 2000;84:390–400. [PubMed: 10899213]

Hoffman KL, Battaglia FP, Harris K, MacLean JN, Marshall L, Mehta MR. The upshot of up states in the neocortex: from slow oscillations to memory formation. J Neurosci 2007;27:11838–11841. [PubMed: 17978020]

Holmgren C, Harkany T, Svennenfors B, Zilberter Y. Pyramidal cell communication within local networks in layer 2/3 of rat neocortex. J Physiol 2003;551:139–153. [PubMed: 12813147]

Hromadka T, Deweese MR, Zador AM. Sparse representation of sounds in the unanesthetized auditory cortex. PLoS Biol 2008;6:e16. [PubMed: 18232737]

Hunter MD, Eickhoff SB, Miller TW, Farrow TF, Wilkinson ID, Woodruff PW. Neural activity in speech-sensitive auditory cortex during silence. Proc Natl Acad Sci USA 2006;103:189–194. [PubMed: 16371474]

Itskov V, Curto C, Harris KD. Valuations for spike train prediction. Neural Comput 2008;20:644–667. [PubMed: 18045025]

Ji D, Wilson MA. Coordinated memory replay in the visual cortex and hippocampus during sleep. Nat Neurosci 2007;10:100–107. [PubMed: 17173043]

Kampa BM, Letzkus JJ, Stuart GJ. Dendritic mechanisms controlling spike-timing-dependent synaptic plasticity. Trends Neurosci 2007;30:456–463. [PubMed: 17765330]

Kaur S, Rose HJ, Lazar R, Liang K, Metherate R. Spectral integration in primary auditory cortex: laminar processing of afferent input, in vivo and in vitro. Neuroscience 2005;134:1033–1045. [PubMed: 15979241]

Kenet T, Bibitchkov D, Tsodyks M, Grinvald A, Arieli A. Spontaneously emerging cortical representations of visual attributes. Nature 2003;425:954–956. [PubMed: 14586468]

Kilgard MP, Merzenich MM. Distributed representation of spectral and temporal information in rat primary auditory cortex. Hear Res 1999;134:16–28. [PubMed: 10452372]

Kimura A, Donishi T, Sakoda T, Hazama M, Tamai Y. Auditory thalamic nuclei projections to the temporal cortex in the rat. Neuroscience 2003;117:1003–1016. [PubMed: 12654352]

Kjaer TW, Hertz JA, Richmond BJ. Decoding cortical neuronal signals: network models, information estimation and spatial tuning. J Comput Neurosci 1994;1:109–139. [PubMed: 8792228]

Kraemer DJ, Macrae CN, Green AE, Kelley WM. Musical imagery: sound of silence activates auditory cortex. Nature 2005;434:158. [PubMed: 15758989]

Laurent G. Olfactory network dynamics and the coding of multidimensional signals. Nat Rev Neurosci 2002;3:884–895. [PubMed: 12415296]

Levy WB, Baxter RA. Energy efficient neural codes. Neural Comput 1996;8:531–543. [PubMed: 8868566]

Liu BH, Wu GK, Arbuckle R, Tao HW, Zhang LI. Defining cortical frequency tuning with recurrent excitatory circuitry. Nat Neurosci 2007;10:1594–1600. [PubMed: 17994013]

Luczak A, Bartho P, Harris KD. Spontaneous events outline the realm of possible sensory reponses in neocortical populations. Neuron 2009;62:413–425. [PubMed: 19447096]

Luczak A, Bartho P, Marguet SL, Buzsaki G, Harris KD. Sequential structure of neocortical spontaneous activity in vivo. Proc Natl Acad Sci USA 2007;104:347–352. [PubMed: 17185420]

MacLean JN, Watson BO, Aaron GB, Yuste R. Internal dynamics determine the cortical response to thalamic stimulation. Neuron 2005;48:811–823. [PubMed: 16337918]

Marr D. A theory of cerebellar cortex. J Physiol 1969;202:437–470. [PubMed: 5784296]

Marr D. Simple memory: a theory for archicortex. Philos Trans R Soc Lond B Biol Sci 1971;262:23–81. [PubMed: 4399412]

Nelson SB, Hempel C, Sugino K. Probing the transcriptome of neuronal cell types. Curr Opin Neurobiol 2006;16:571–576. [PubMed: 16962313]

Ojima H, Honda CN, Jones EG. Characteristics of intracellularly injected infragranular pyramidal neurons in cat primary auditory cortex. Cereb Cortex 1992;2:197–216. [PubMed: 1511221]

Olshausen BA, Field DJ. Sparse coding of sensory inputs. Curr Opin Neurobiol 2004;14:481–487. [PubMed: 15321069]

Oswald AM, Reyes AD. Maturation of intrinsic and synaptic properties of layer 2/3 pyramidal neurons in mouse auditory cortex. J Neurophysiol 2008;99:2998–3008. [PubMed: 18417631]

Paxinos, G.; Watson, C. The Rat Brain in Stereotaxic Coordinates. San Diego: Academit Press; 1997.

Petersen CC, Hahn TT, Mehta M, Grinvald A, Sakmann B. Interaction of sensory responses with spontaneous depolarization in layer 2/3 barrel cortex. Proc Natl Acad Sci USA 2003;100:13638–13643. [PubMed: 14595013]

Pinault D. A novel single-cell staining procedure performed in vivo under electrophysiological control: morpho-functional features of juxtacellularly labeled thalamic cells and other central neurons with biocytin or Neurobiotin. J Neurosci Methods 1996;65:113–136. [PubMed: 8740589]

Poulet JF, Petersen CC. Internal brain state regulates membrane potential synchrony in barrel cortex of behaving mice. Nature 2008;454:881–885. [PubMed: 18633351]

Quiroga RQ, Reddy L, Kreiman G, Koch C, Fried I. Invariant visual representation by single neurons in the human brain. Nature 2005;435:1102–1107. [PubMed: 15973409]

Rieke, F.; Warland, D.; de Ruyter van Steveninck, RR.; Bialek, W. Spikes: Exploring the neural code. Cambridge: The MIT Press; 1997.

Romanski LM, LeDoux JE. Organization of rodent auditory cortex: anterograde transport of PHA-L from MGv to temporal neocortex. Cereb Cortex 1993;3:499–514. [PubMed: 7511011]

Rouiller EM, Simm GM, Villa AE, de Ribaupierre Y, de Ribaupierre F. Auditory corticocortical interconnections in the cat: evidence for parallel and hierarchical arrangement of the auditory cortical areas. Exp Brain Res 1991;86:483–505. [PubMed: 1722171]

Sanchez-Vives MV, McCormick DA. Cellular and network mechanisms of rhythmic recurrent activity in neocortex. Nat Neurosci 2000;3:1027–1034. [PubMed: 11017176]

Schmitzer-Torbert N, Jackson J, Henze D, Harris K, Redish AD. Quantitative measures of cluster quality for use in extracellular recordings. Neuroscience 2005;131:1–11. [PubMed: 15680687]

Schreiner CE, Read HL, Sutter ML. Modular organization of frequency integration in primary auditory cortex. Annu Rev Neurosci 2000;23:501–529. [PubMed: 10845073]

Schubert D, Kotter R, Staiger JF. Mapping functional connectivity in barrel-related columns reveals layer- and cell type-specific microcircuits. Brain Struct Funct 2007;212:107–119. [PubMed: 17717691]

Simons DJ. Response properties of vibrissa units in rat SI somatosensory neocortex. J Neurophysiol 1978;41:798–820. [PubMed: 660231]

Sirota A, Montgomery S, Fujisawa S, Isomura Y, Zugaro M, Buzsaki G. Entrainment of neocortical neurons and gamma oscillations by the hippocampal theta rhythm. Neuron 2008;60:683–697. [PubMed: 19038224]

Smith PH, Populin LC. Fundamental differences between the thalamocortical recipient layers of the cat auditory and visual cortices. J Comp Neurol 2001;436:508–519. [PubMed: 11447593]

Sohya K, Kameyama K, Yanagawa Y, Obata K, Tsumoto T. GABAergic neurons are less selective to stimulus orientation than excitatory neurons in layer II/III of visual cortex, as revealed by in vivo functional Ca2+ imaging in transgenic mice. J Neurosci 2007;27:2145–2149. [PubMed: 17314309]

Steriade M, Nunez A, Amzica F. A novel slow (< 1 Hz) oscillation of neocortical neurons in vivo: depolarizing and hyperpolarizing components. Journal of Neuroscience 1993;13:3252–3265. [PubMed: 8340806]

Swadlow HA. Efferent neurons and suspected interneurons in binocular visual cortex of the awake rabbit: receptive fields and binocular properties. J Neurophysiol 1988;59:1162–1187. [PubMed: 3373273]

Swadlow HA. Efferent neurons and suspected interneurons in S-1 vibrissa cortex of the awake rabbit: receptive fields and axonal properties. J Neurophysiol 1989;62:288–308. [PubMed: 2754479]

Swadlow HA. Efferent neurons and suspected interneurons in motor cortex of the awake rabbit: axonal properties, sensory receptive fields, and subthreshold synaptic inputs. J Neurophysiol 1994;71:437–453. [PubMed: 8176419]

Szentagothai J. The modular architectonic principle of neural centers. Rev Physiol Biochem Pharmacol 1983;98:11–61. [PubMed: 6361964]

Thomson AM, Lamy C. Functional maps of neocortical local circuitry. Frontiers in Neuroscience 2007;1:19–42. [PubMed: 18982117]

Timofeev I, Grenier F, Bazhenov M, Sejnowski TJ, Steriade M. Origin of slow cortical oscillations in deafferented cortical slabs. Cereb Cortex 2000;10:1185–1199. [PubMed: 11073868]

Turner JG, Hughes LF, Caspary DM. Divergent response properties of layer-V neurons in rat primary auditory cortex. Hear Res 2005;202:129–140. [PubMed: 15811705]

van Brederode JF, Spain WJ. Differences in inhibitory synaptic input between layer II–III and layer V neurons of the cat neocortex. J Neurophysiol 1995;74:1149–1166. [PubMed: 7500140]

Vinje WE, Gallant JL. Sparse coding and decorrelation in primary visual cortex during natural vision. Science 2000;287:1273–1276. [PubMed: 10678835]

Wallace MN, Palmer AR. Laminar differences in the response properties of cells in the primary auditory cortex. Exp Brain Res 2008;184:179–191. [PubMed: 17828392]

Wang X, Lu T, Bendor D, Bartlett E. Neural coding of temporal information in auditory thalamus and cortex. Neuroscience 2008;154:294–303. [PubMed: 18555164]

Willmore B, Tolhurst DJ. Characterizing the sparseness of neural codes. Network 2001;12:255–270. [PubMed: 11563529]

Winer JA, Lee CC. The distributed auditory cortex. Hear Res 2007;229:3–13. [PubMed: 17329049]

Wu GK, Arbuckle R, Liu BH, Tao HW, Zhang LI. Lateral sharpening of cortical frequency tuning by approximately balanced inhibition. Neuron 2008;58:132–143. [PubMed: 18400169]

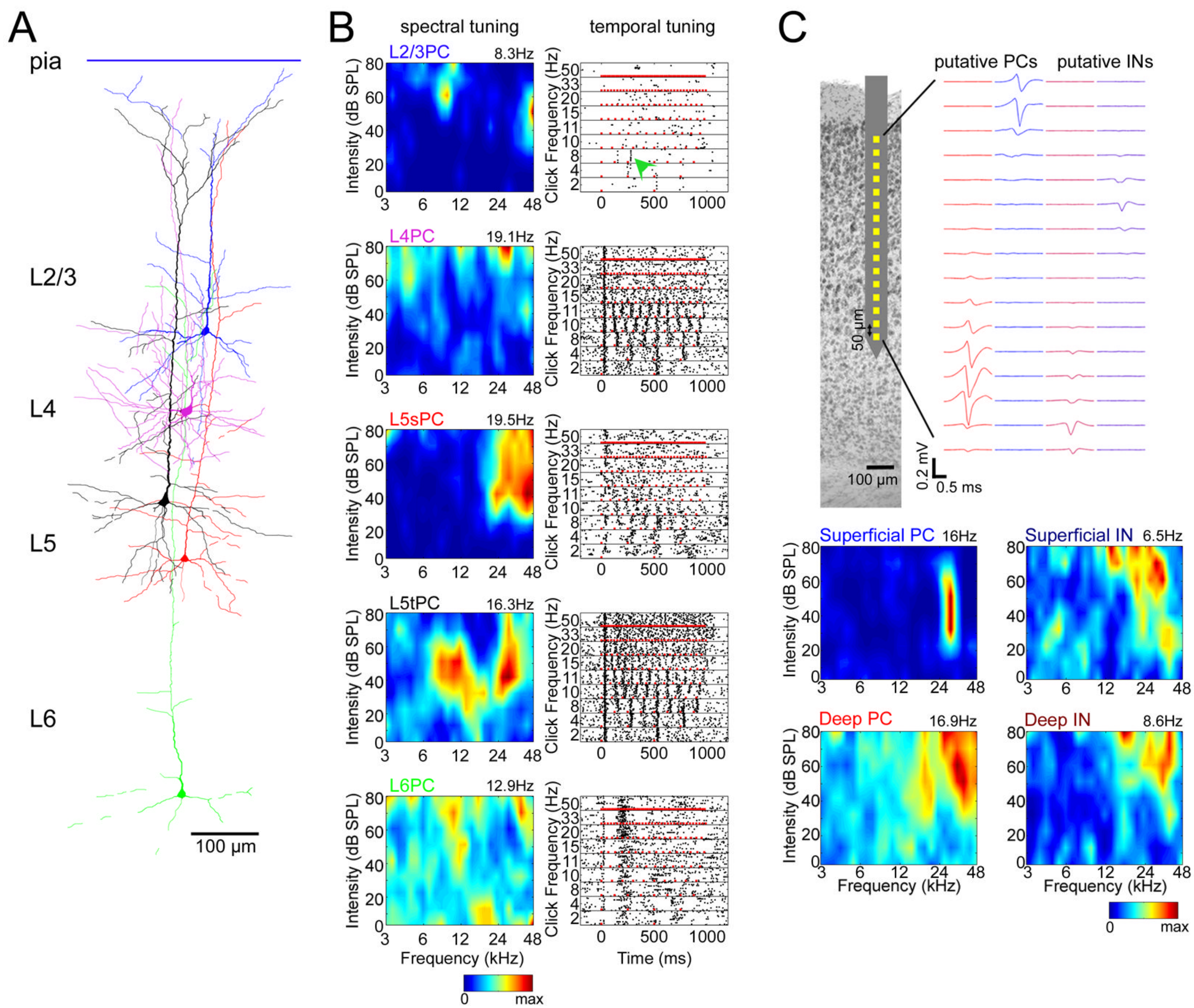

Figure 1. Tuning profiles of example neurons

(**A**) Examples of five juxtacellularly recorded pyramidal cells (PCs), digitally superimposed. (**B**) Spectral and temporal tuning of the neurons shown in (A). *Left*, responses to pure tones. Each plot shows a pseudocolor representation of the cell s mean firing rate in a 50ms period following tone onsets, as a function of tone frequency and intensity. The number above each plot indicates maximum firing rate. *Right*, responses to click trains. Each plot shows a raster representation of the cell s response to repeated presentations of click trains of varying frequencies. Red marks indicate click (5-ms white noise) onsets. Green arrowhead: the example L2/3 PC responded sparsely to click train stimuli, with reliable firing seen only to the 3rd click of an 8Hz train. L5sPC, L5 slender PC; L5tPC, L5 thick PC.

(**C**) Tuning of four representative cells identified from silicon probe recordings. *Top*, schematic drawing of electrode, and average spike waveform profiles of a putative deep PC, superficial PC, deep interneuron(IN), and superficial IN. *Bottom*, spectral tuning of these cells.

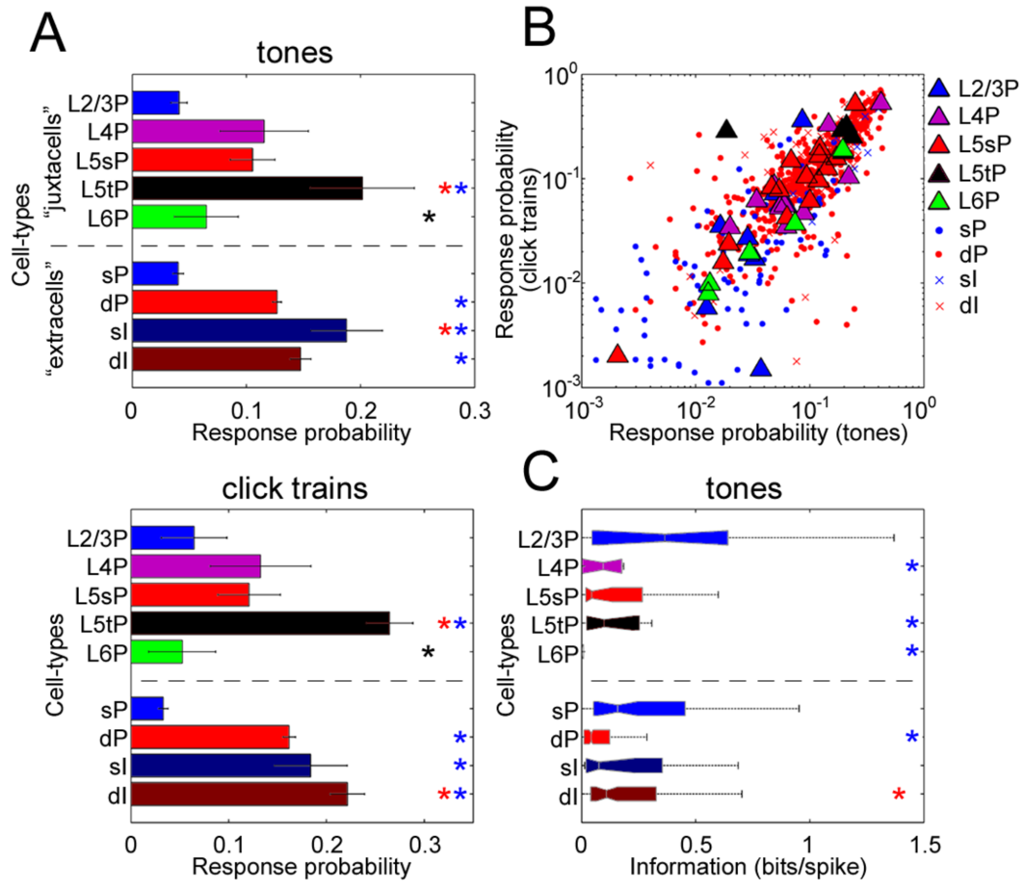

Figure 2. Sparseness of sensory responses varies between cell classes

(**A**) Sparseness was assessed using a "response probability" measure, for which smaller values indicate sparser firing (see text). Bars above and below dotted line indicate cell-classes identified morphologically by juxtacellular recording ("juxtacells"), and silicon probe-recorded units putatively classified by spike waveform ("extracells"), respectively. Asterisks denote pairwise post-hoc lsd tests, indicating a significant difference ($p<0.05$) to the class corresponding to that color. Post-hoc comparisons were performed for juxtacells and extracells separately. sP, superficial PCs; dP, deep PCs; sI, superficial INs; dI, deep INs. Error bars indicate SE.

(**B**) Sparseness is correlated across stimulus types. Each symbol shows the response probability of one cell to tone and click stimuli, with large symbols indicating juxtacells.

(**C**) Information-theoretic analysis. L2/3PCs showed greater predictability from the presented tone, measured in bits/spike, than L4PCs, L5tPCs and L6PCs (ANOVA with post-hoc lsd test, $p<0.01$).

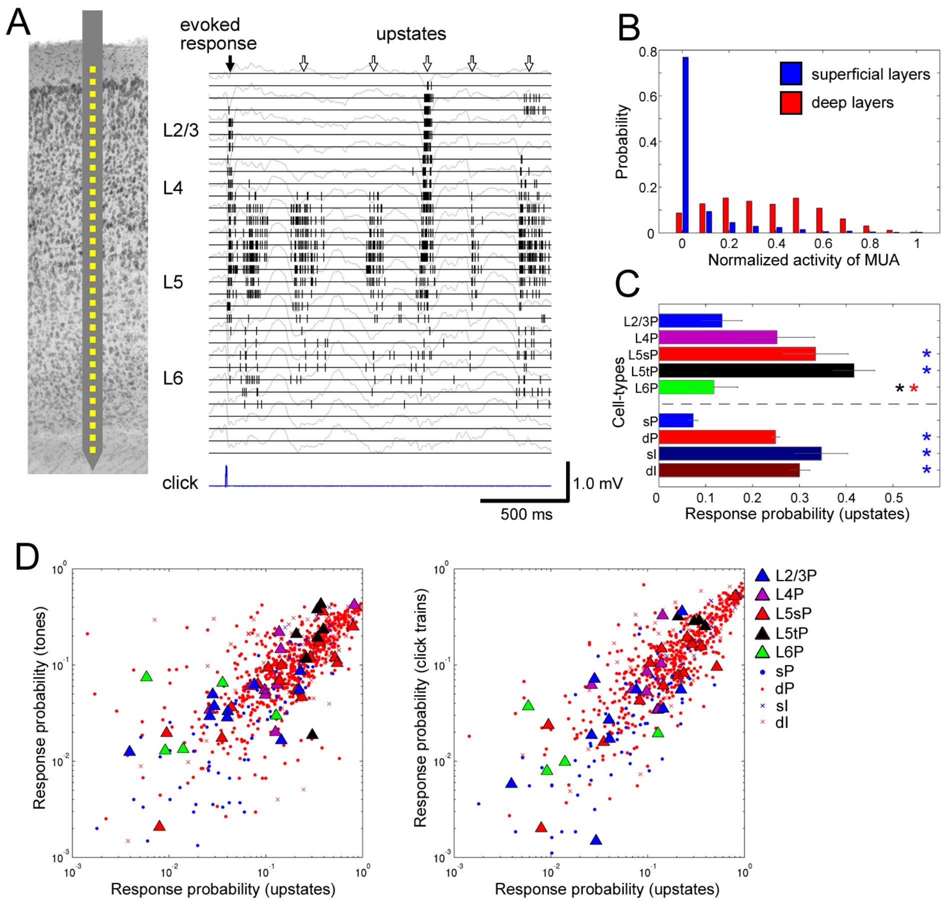

Figure 3. Sparseness varies between cell classes during spontaneous activity

(**A**) *Left*, schematic drawing of recording by a 32-site linear electrode. *Right*, raster plot of multi-unit activity (MUA) for each channel, superimposed on local-field potentials (gray traces).

(**B**) Probability distributions of normalized MUA spike count across upstates, for superficial (putative L2/3) and deep (putative L5) layers (2082 upstates from 5 datasets). Distribution of superficial MUA differs significantly from that of deep layers (Kolmogorov-Smirnov test, p<0.0001).

(**C**) Response probability measure of firing sparseness for upstates, for all cell types (c.f. Figure 2A).

(**D**) Correlation of response probability between sensory responses and upstates (c.f. Figure 2B).

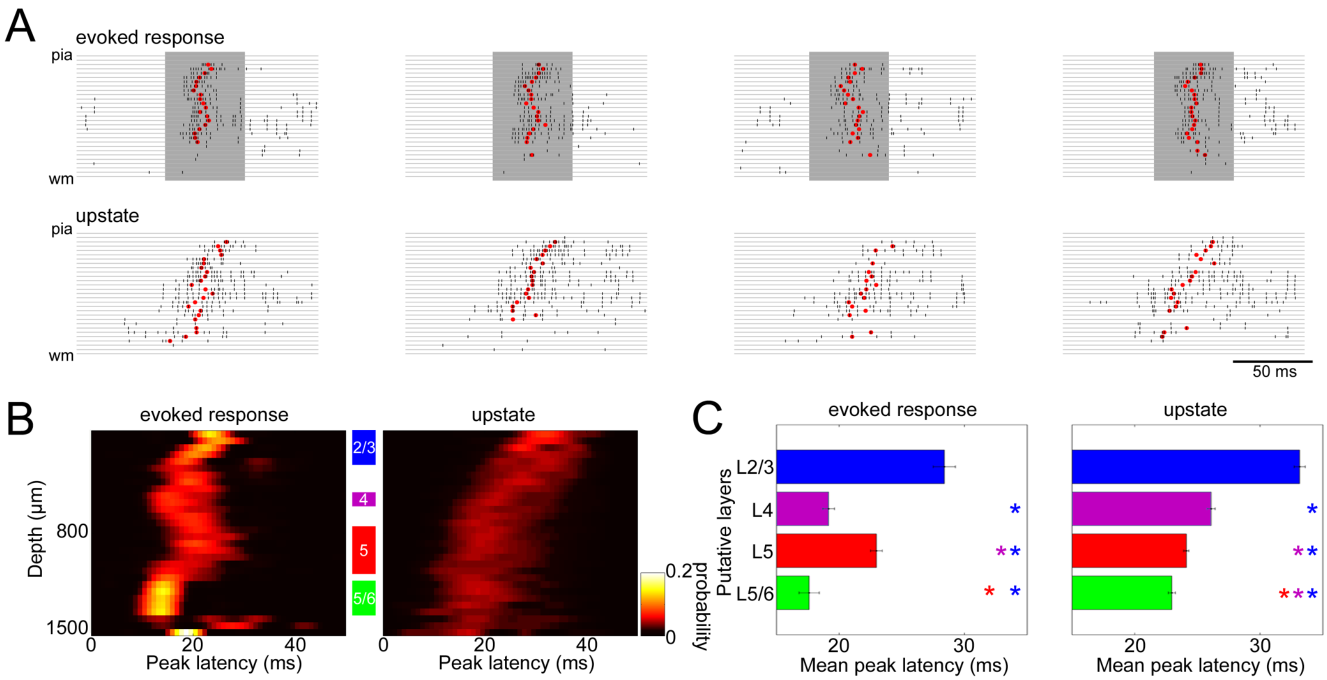

Figure 4. Spread of activity across layers differs between sensory responses and upstates

(**A**) Example laminar profiles of upstates and evoked responses. Rasters indicate MUA of all channels on a 32-site linear probe for individual upstates and evoked responses. Shaded periods indicate tone presentations. Red dots indicate "peak latency," computed as the median MUA spike time in a 50-ms window after event onset.

(**B**) Laminar profiles of peak latency for tone-evoked responses (best frequency, 60–80 dB SPL) and upstates. The graphs show a pseudocolor histogram of the distribution of peak latency as a function of depth, revealing temporal sequence of activity across layers. Data accumulated from all experiments with 32-site linear probes (N=5).

(**C**) Statistical summary of peak latency for putative layers corresponding to the shaded areas in (B). Each bar shows mean and SE of peak latency measure across all experiments. For evoked responses, activity started in putative L4 and the L5/6 border. For upstates, activity started in deep layers. Colored asterisks indicate significant post-hoc comparisons (lsd test, $p<0.05$).

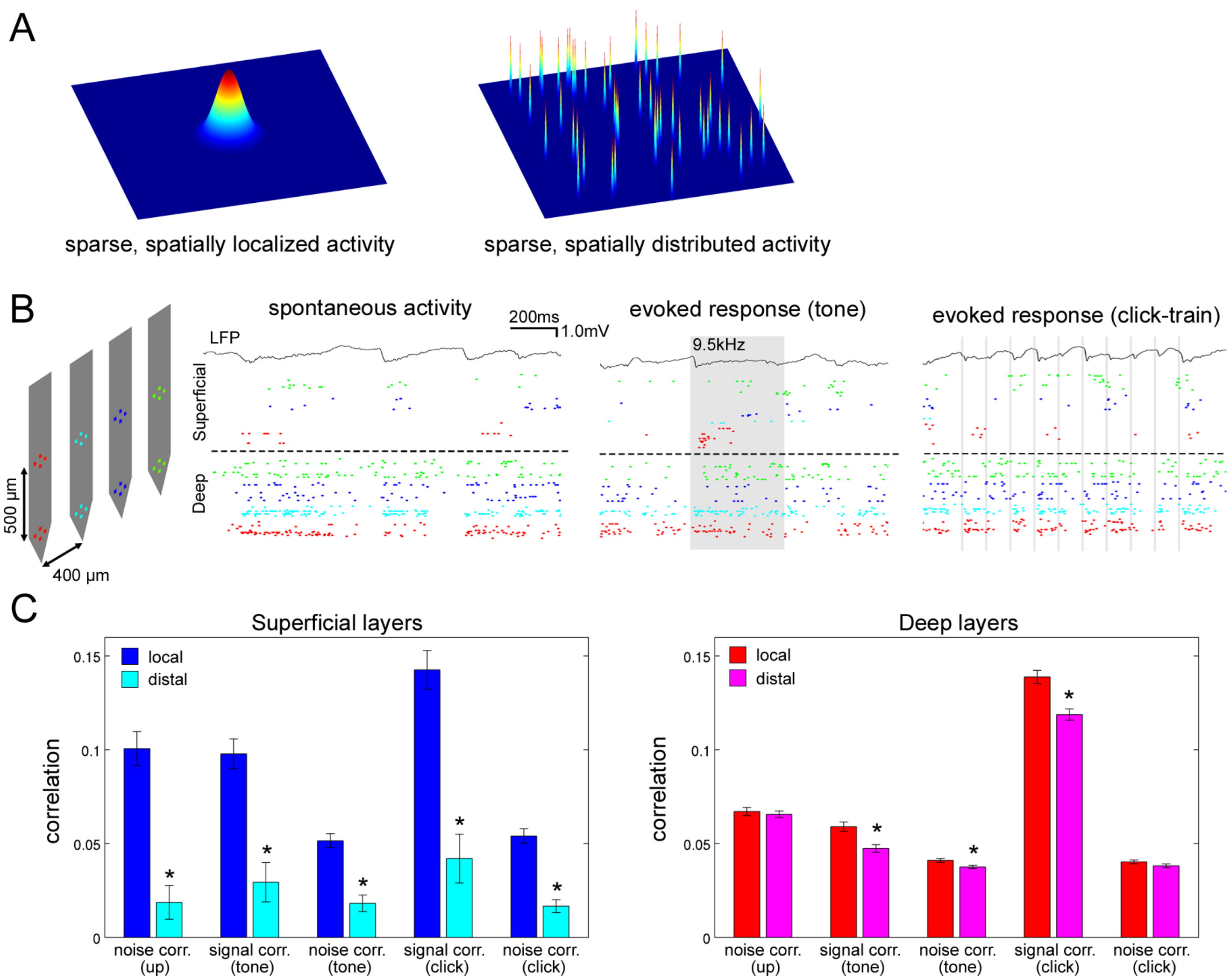

Figure 5. Laminar-dependent structure of correlated activity

(**A**) Two possible models for sparse population activity. *Left*, sparse, spatially localized model; *right*, sparse, spatially distributed model.

(**B**) Example extracellular recordings spanning multiple columns. *Left*, Probe configuration. *Right*, Spontaneous and sensory-evoked activity of simultaneously recorded cells. Rasters above and below the dashed line correspond to recording sites in superficial (putative L2/3) and deep (putative L5) layers, respectively. Colors of each raster correspond to colors of recording sites in schematic. Shaded areas denote periods of tone and click presentations.

(**C**) Spatial dependence of spike count correlation in superficial (*left*) and deep (*right*) layers. Asterisks indicate significant post-hoc comparisons (lsd test, $p<0.05$). Error bars indicate SE.

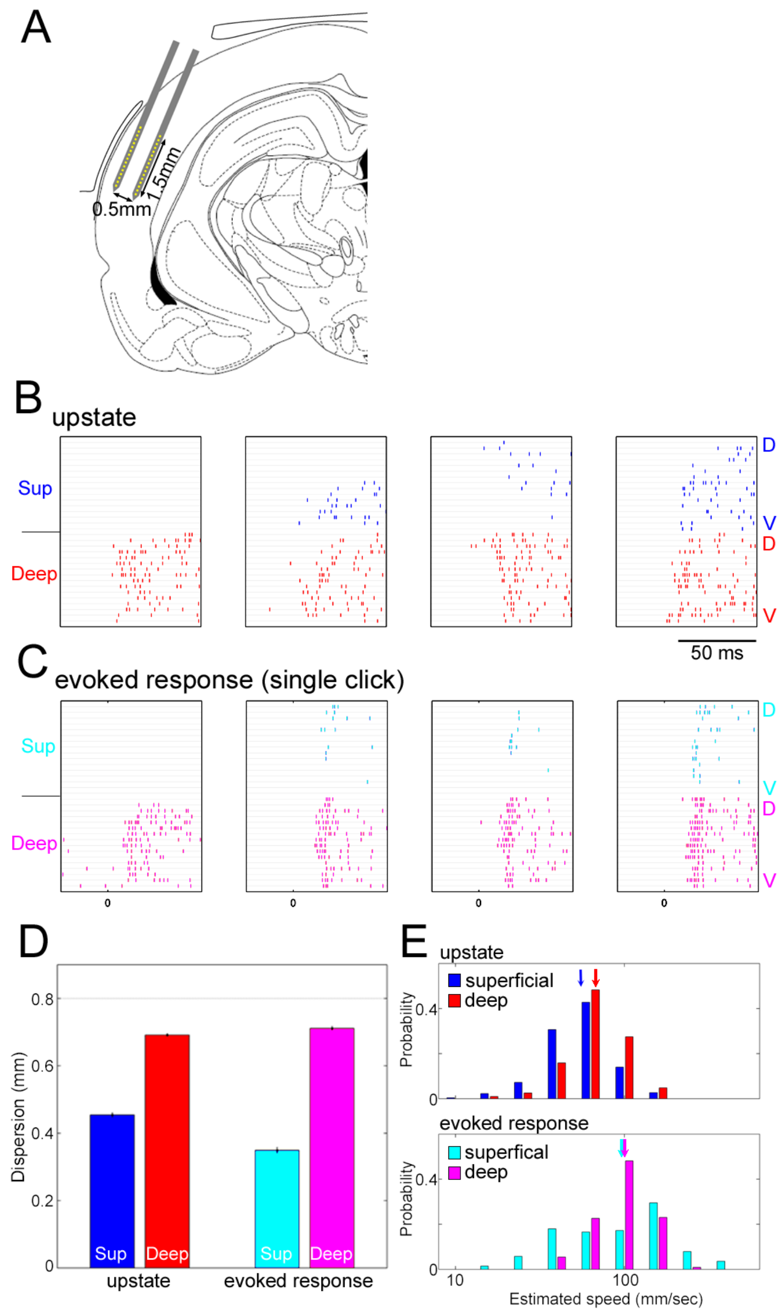

Figure 6. Spatiotemporal dispersion of population activity

(**A**) Two-shank multisite electrodes (2×16 linear probe) were inserted parallel to the layers of auditory cortex. A part of the drawing was replicated from (Paxinos and Watson, 1997). (**B,C**) Examples of spatiotemporal patters for upstates (**B**) and click-evoked responses (**C**). Each plot shows rasters of MUA on all recording sites, with superficial and deep shanks on top and bottom. The sites on each shank are arranged from dorsal (D) to ventral (V). Superficial activity was sparse and local for both types of event. While upstates sometimes spread as a traveling wave, evoked responses typically appeared with near-synchrony across columns. (**D**) Dispersion of activity was quantified by the spatial inter-quartile range of MUA spike counts across recording sites in a 50ms window after event onset (see **Experimental**

Procedures). Dispersion in superficial layers was restricted compared to that in deep layers (ANOVA with post hoc lsd test, $p<0.0001$). Error bars indicate SE.

(**E**) Distribution of propagation speeds for upstates (*top*) and evoked responses (*bottom*), estimated as the regression slope of median MUA time across recording sites (Luczak et al., 2007; see also Figure S13). Arrows indicate the median, and the x-axis is log-scaled. Propagation speed was faster for evoked responses than for upstates in both layers (ANOVA with post hoc lsd test, $p<0.0001$).

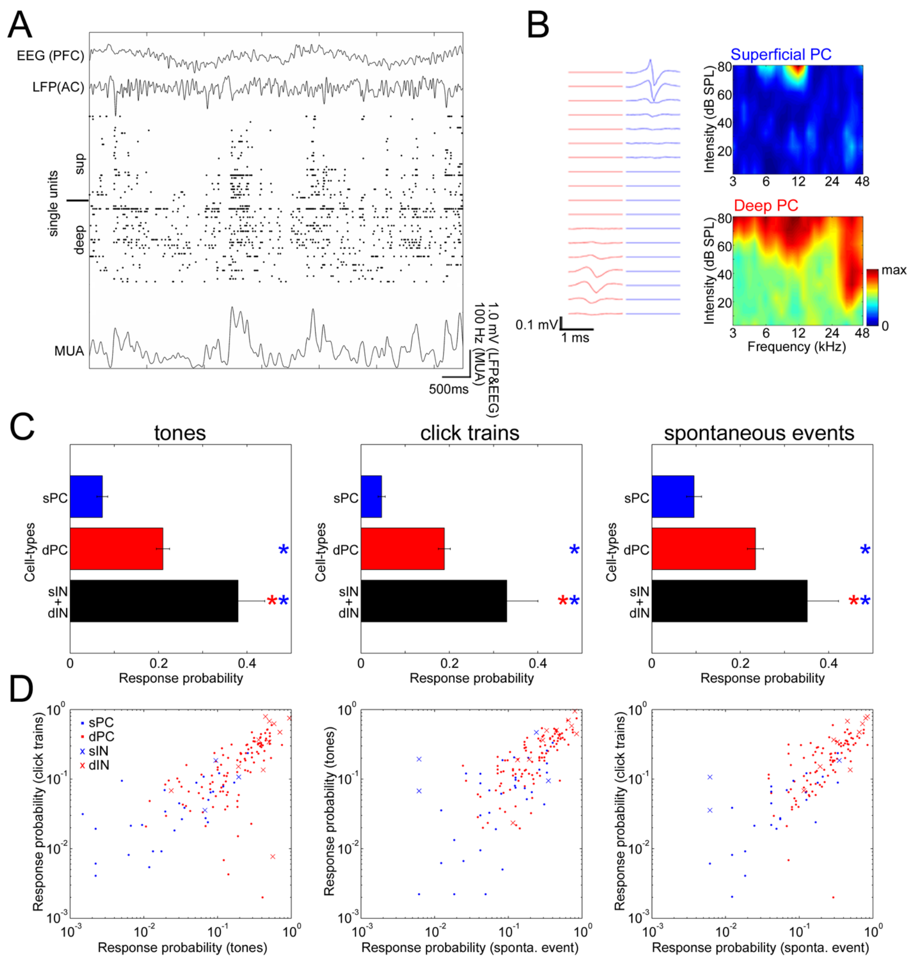

Figure 7. Cell-type dependent sparseness of spontaneous and evoked activity in unanesthetized animals

(**A**) Raster of simultaneously recorded spike-sorted units showing spontaneous fluctuations of population activity in a head-restrained, unanesthetized animal. Also shown are electroencephalogram (EEG) recorded from the prefrontal cortical (PFC) area with a screw, local-field potential (LFP) recorded locally (AC, auditory cortex), and multiunit activity (MUA), calculated by summation of firing of all single units and smoothing with a 70-ms Gaussian kernel.

(**B**) *Left*, example waveform profiles of simultaneously recorded putative superficial and deep PCs. *Right*, spectral tuning of example cells.

(**C**) Response probabilities of extracellularly recorded cells for tones (left), click trains (center), and spontaneous events (*right*), indicating sparser activity of superficial putative PCs than those of deep putative PCs and putative INs (ANOVA with post hoc lsd test, p<0.0001 in all cases) (c.f. Figures 2A and 3C). Asterisks denote pairwise post-hoc lsd tests, indicating a significant difference (p<0.05) to the class corresponding to that color. sP, superficial PCs; dP, deep PCs; sI, superficial INs; dI, deep INs. Error bars indicate SE.

(**D**) Sparseness is correlated across event types (r=0.80, p<0.0001 in *left;* r=0.73, p<0.0001 in *center;* r=0.72, p<0.0001 in *right*). Each symbol shows the response probability of one cell to tone and click stimuli (*left*), tone stimuli and spontaneous events (*center*), and click stimuli and spontaneous events (*right*) (c.f. Figures 2C and 3D).

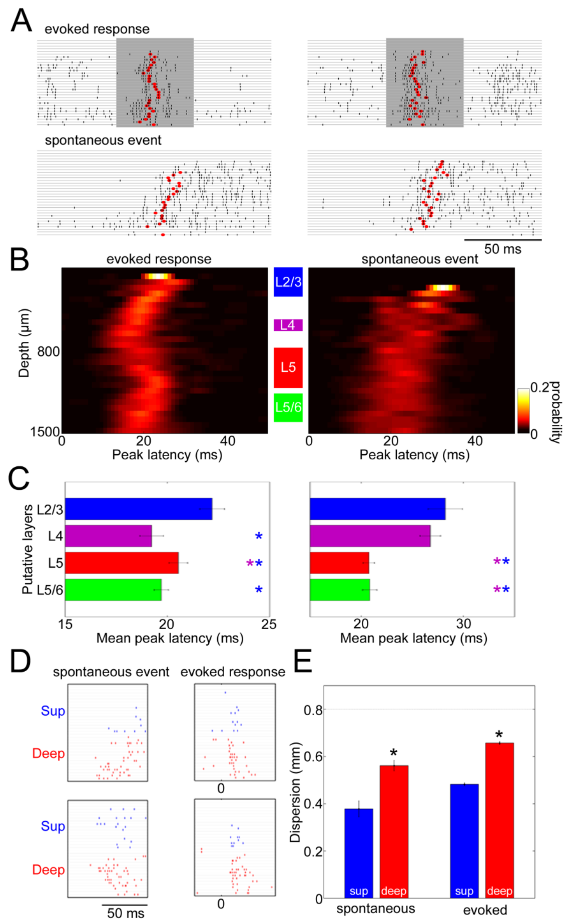

Figure 8. Spatiotemporal structure of evoked and spontaneous activity in unanesthetized animals

(**A**) Example laminar MUA rasters for evoked responses and spontaneous events (c.f. Figure 4A).

(**B**) Laminar profiles of peak latency for tone-evoked responses and spontaneous events. The graphs show a pseudocolor histogram of the distribution of peak latency as a function of depth, revealing temporal sequence of activity across layers. Data accumulated from all experiments with 32-site linear probes (N=5; c.f. Figure 4B).

(**C**) Laminar profiles of mean peak latency (5 datasets; c.f. Figure 4C). Colored asterisks indicate significant post-hoc comparisons (p<0.05). Error bars indicate SE.

(**D**) Example spatiotemporal patters for spontaneous events and click-evoked responses recorded by two-shank multisite electrodes (c.f. Figures 6A–C).

(**E**) Spatial dispersion of activity (c.f. Figure 6D). Error bars indicate SE.

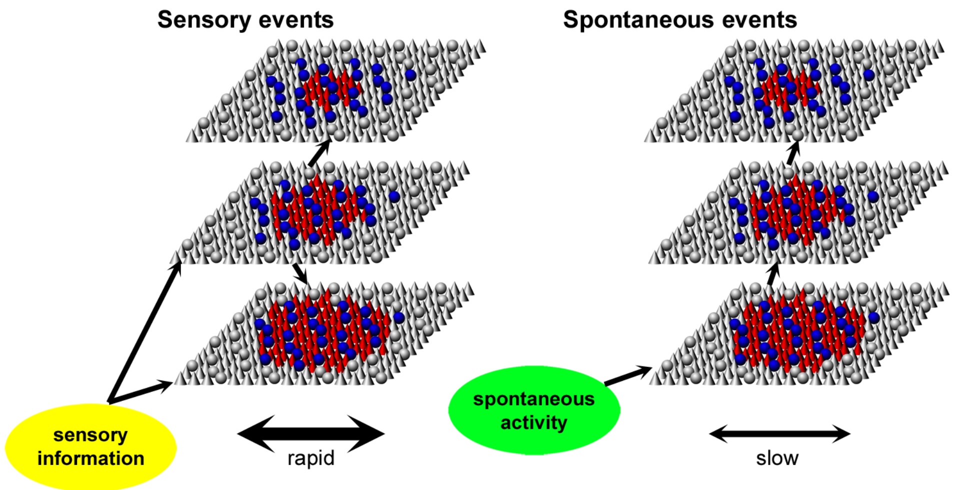

Figure 9. Hypothesized flow of sensory-evoked and spontaneous activity through auditory cortical circuits

Each sheet represents a population of the corresponding layer, with cones and spheres representing PCs and INs, respectively. Colored symbols represent active neurons. For both types of activity, pyramidal cells exhibited dense and distributed activity in the deep layers, but sparse and localized activity in the superficial layers; interneurons show a pattern of activity similar to that of deep layer pyramidal cells. For sensory responses, earliest firing is seen in cells of the middle and deep layers, presumably reflecting the strongest afferent input onto these neurons. For spontaneous events, activity spread upward from the deep layers.